

# Rolling SLIP: a Model for Running Locomotion with Rolling Contact

Ke-Jung Huang and Pei-Chun Lin

**Abstract**—We report on the development of the model for running locomotion with rolling contact, R-SLIP, to simulate the motion of the robot with circular legs. Thus, two significant characteristics which cannot be correctly modeled in the traditional SLIP, rolling contact with varied equivalent linear spring during locomotion, can be adequately captured. The stability of the R-SLIP model was analyzed numerically by varying the factors which affects the dynamic performance of the model, including stiffness of the torsion spring, touchdown angle, touchdown speed, and landing angle. In addition, the return map was utilized to check the state transition of the touchdown angle with given other three factors. The results reveal that the R-SLIP model has self-stable gaits, just like the traditional SLIP. Thus, with adequate initial conditions and system parameters, the model can run stably around the fixed point without control effort.

## I. INTRODUCTION

The natural environment is in general rough and diversified. After a long evolution process, most ground animals are evolved with agile and robust legs, and these legs are capable of allowing animals to move elegantly and rapidly over uneven terrain. Though geometrical configurations and evolved stages of the legs vary significantly, researchers found that through the adequate motion coordination among the legs, animals' dynamic locomotion in the sagittal plane can be approximated by a simple mathematical model "SLIP" (Spring-Loaded Inverted Pendulum) [1-3], where the body is treated as a point mass and the legs are approximated by a massless spring. The SLIP model is energy conservative; however, it is widely recognized as the intrinsic and qualitative representation of the ground animals' running behavior. As a running "template", SLIP model indeed provides a prescriptive control guidance [4, 5] to the original complex biological or robotic systems which represents empirical "anchors" by sketching the actuation joints and rigid structures [6]. Thus, in the past few decades the successfulness of the dynamic behavior development of the legged robots is roughly judged by the similarity of the robot's motion characteristics to that of the SLIP model, which in general has the potential and kinetic energy exchange as well as has the aerial phase during locomotion.

The study of dynamic robotic systems was initiated by the development of monopods in the 80s [7], and following that

This work is supported by National Science Council (NSC), Taiwan, under contract 100-2628-E-002 -021-MY3 and by National Taiwan University (NTU) under contract 10R70817.

Authors are with Department of Mechanical Engineering, National Taiwan University (NTU), No.1 Roosevelt Rd. Sec.4, Taipei, Taiwan. (Corresponding email: peichunlin@ntu.edu.tw).

various quadruped and hexapod robots were reported. For example, the Scout series [8], Tekken series [9], Sprawl series [10-12], RHex [13, 14], etc. In addition, the dynamical climbing robot has been reported as well [15]. Possibly owing to the limited power density of commercial motors, the excitation of the dynamical behaviors of current robots mostly relies on the adequately allocation of compliant parts which can store and release potential energy in the right timings. For example, the hexapod RHex has only one rotational degree of freedom (DOF) per leg, but it can easily generate SLIP-like jogging behavior with its compliant legs [16, 17]. In addition, it also has great ability to negotiate rough terrain owing to the strategy of full-rotation leg reposition. The hexapod iSprawl has carefully tuned leg compliance, and it can be driven by a single motor and generates SLIP-like locomotion [10].

However, empirical evaluation reveals that design and fabrication of the ideal linear spring with strong resistance to the lateral force is challenge. In contrast, it is feasible to fabricate and form compliant material into circular shape. Thus, this type of legs is adopted in many robot designs [18], and hereafter it is referred to as the "circular leg." The circular leg has two significant intrinsic characteristics different than those of the traditional SLIP model. First, instead of point ground-contact, the ground-contact of the circular leg exhibits rolling behavior, and the ground-contact point gradually shifts forward during motion. Second, owing to the rolling contact, the compliance of the leg simultaneously changes during motion. Thus, a new dynamic template is desired to model the behavior of the circular leg. A two-segment model with point-contact [19] as well as an ordinary SLIP with a small rolling foot (SLIP-R) [20] have been studied before. However, these two models cannot capture two characteristics described above. Considering those characteristics, here we propose a new *SLIP model with rolling behavior* (i.e., referred to as R-SLIP) to simulate the motion of circular leg.

Section II describes the proposed R-SLIP model, and Section III reports the dynamics of the model. Section IV concludes the work.

## II. ROLLING SLIP MODEL

The compliant circular leg exhibits the rolling behavior between the leg and the ground, and this characteristics deviates the behavior of the robot locomotion away from the traditional SLIP model with point ground on two prospects: (i) the equivalent linear leg stiffness varies while the ground contact point changes; (ii) the rolling motion yields the forward movement of the robot body. To realistically take

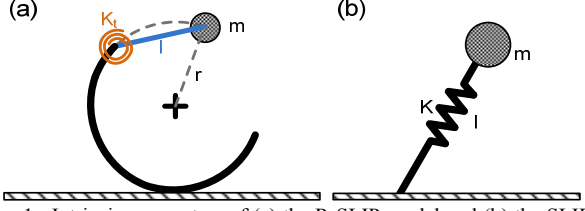


Fig. 1. Intrinsic parameters of (a) the R-SLIP model and (b) the SLIP model.

these two characteristics into account, a modified SLIP model named R-SLIP is developed as shown in Fig. 1(a). It has two segments connected by a torsion spring. The lower rigid segment is part of a circular rim, thus representing the original rolling behavior of the circular leg. The spring constant of the torsion spring is assumed fixed. The upper rigid segment connecting the torsion spring and a point mass. When the spring is in its natural configuration, the mass is located on the circular rim as well (i.e., with the same distance to the center of the circular rim as the radius of the circular rim). Therefore, the R-SLIP has four intrinsic parameters: radius of the circular rim ( $r$ ), stiffness of the torsion spring ( $K_t$ ), mass ( $m$ ), and the distance between the torsion spring and the mass ( $l$ ) as shown in Fig. 1(a). In contrast, the traditional SLIP has three parameters: length of the spring, stiffness of the spring, and mass as shown in Fig. 1(b).

The qualitative behavior of the R-SLIP model likes that of the compliant circular leg. When the R-SLIP model rolls on the ground, because the distance between the ground-contact point and the torsion spring changes accordingly, the equivalent linear stiffness changes, which is defined by the stiffness along with the direction of the ground-contact point and the mass. Therefore, the compliance change in the circular leg during its motion can be modeled in the R-SLIP as well.

Like the traditional SLIP model, a full running stride of the R-SLIP model can be divided into stance phase and flight phase as shown in Fig. 2(a). In the flight phase, the R-SLIP moves according to ballistic model, affected by the gravity only. With pre-determined landing angle  $\beta$ , when the height of the mass to the ground is less than  $r + rsin(\beta)$ , the touchdown occurs and the stance phase begins. Owing to the landing momentum, the R-SLIP model rolls on the ground and the torsion spring is compressed simultaneously. At certain moment the spring starts uncompressing. When the torsion spring returns to its natural configuration, the R-SLIP model lift-offs and the flight phase begins. If the R-SLIP moves stably, the motion is composed of these two phases and switched periodically.

The dynamic behavior of the R-SLIP model in the stance phase can be constructed by the Lagrangian method. The angles  $\theta$  and  $\phi$  are utilized as the generalized coordinate and are depicted in Fig. 2(b). The angle  $\theta$  is defined as the angle included by the horizontal line and the line segment connecting the torsion spring and the mass,  $l$ . The angle  $\phi$  represents the compression level of the torsion spring, and it

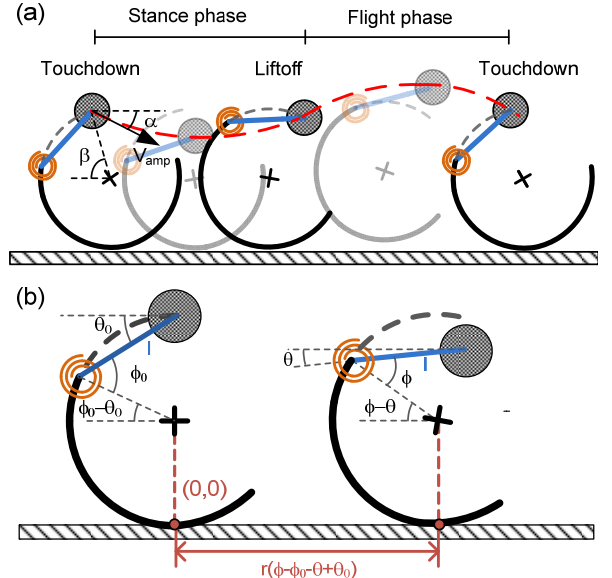


Fig. 2. The R-SLIP model: (a) illustrative sketch of its running motion with stance phase and flight phase. The variables for defining the touchdown state is also presented. (b) the parameters utilized in the development of the modified SLIP model.

is defined as the angle included by  $l$  and the line connecting the torsion spring and the center of the circular rim. Following these definitions, the Cartesian coordinates of the mass in the stance phase,  $(x_s, y_s)$ , can be represented as

$$x_s = r(\phi - \phi_0 - \theta + \theta_0) - r \cos(\phi - \theta) + l \cos(\theta) \quad (1)$$

where the subscripts  $s$  of  $(x, y)$  and 0 of  $\theta$  and  $\phi$  indicate the stance phase and natural configuration, respectively. The velocity state can then be derived as

$$\dot{x}_s = r(1 + \sin(\phi - \theta))(\dot{\phi} - \dot{\theta}) - l \sin(\theta)\dot{\theta} \quad (2)$$

$\dot{y}_s = r \cos(\phi - \theta)(\dot{\phi} - \dot{\theta}) + l \cos(\theta)\dot{\theta}$ . Following (1) and (2), the kinetic energy  $T$  can be formulated as

$$T = m\{r^2[1 + \sin(\phi - \theta)](\dot{\phi} - \dot{\theta})^2 + rl(\cos(\phi) - \sin(\theta))(\dot{\phi}\dot{\theta} - \dot{\theta}^2) + \frac{1}{2}l^2\dot{\theta}^2\}, \quad (3)$$

and the potential energy  $V$  is

$$V = \frac{1}{2}K_t(\phi_0 - \phi)^2 + mg(r + rsin(\phi - \theta) + lsin(\theta)), \quad (4)$$

which includes gravitational and elastic potential energies. Assuming the rolling motion is pure without sliding, the ground reacting force does not contribute. Therefore, the energy of the system is conservative and the following equations are held

$$\begin{aligned} \frac{d}{dt}\left(\frac{\partial T}{\partial \dot{\theta}}\right) - \frac{\partial T}{\partial \theta} + \frac{\partial V}{\partial \theta} &= 0 \\ \frac{d}{dt}\left(\frac{\partial T}{\partial \dot{\phi}}\right) - \frac{\partial T}{\partial \phi} + \frac{\partial V}{\partial \phi} &= 0. \end{aligned} \quad (5)$$

By importing (3) and (4), equation (5) can be expressed as

$$m\left(\begin{aligned} &(2r^2(1 + \sin(\phi - \theta)) - 2rl(\cos(\phi) - \sin(\theta)) + l^2)\ddot{\theta} \\ &+ (-2r^2(1 + \sin(\phi - \theta)) + rl(\cos(\phi) - \sin(\theta)))\ddot{\phi} \\ &+ \left(-r^2 \cos(\phi - \theta)(\dot{\phi} - \dot{\theta})^2 - rlsin(\phi)(\dot{\phi}^2 - 2\dot{\phi}\dot{\theta}) + rlcos(\theta)\dot{\theta}^2\right) \\ &+ g(lcos(\theta) - rcos(\phi - \theta)) \end{aligned}\right) = 0$$

$$m \left( \begin{array}{c} (-2r^2(1 + \sin(\theta - \phi)) + rl(\cos(\theta) - \sin(\theta)))\ddot{\phi} \\ +(2r^2(1 + \sin(\theta - \phi)))\dot{\phi} \\ + \left( r^2 \cos(\theta - \phi) (\dot{\phi} - \dot{\theta})^2 - rl(\sin(\theta) + \cos(\theta))\dot{\theta}^2 \right) \\ + gr\cos(\theta - \phi) \end{array} \right) - K_t(\phi_0 - \phi) = 0. \quad (6)$$

And (6) can be expressed as

$$\begin{bmatrix} a1(\theta, \phi) & b1(\theta, \phi) \\ a2(\theta, \phi) & b2(\theta, \phi) \end{bmatrix} \begin{bmatrix} \ddot{\theta} \\ \ddot{\phi} \end{bmatrix} = \begin{bmatrix} c1(\theta, \phi, \dot{\theta}, \dot{\phi}) \\ c2(\theta, \phi, \dot{\theta}, \dot{\phi}) \end{bmatrix}$$

$$\begin{bmatrix} \ddot{\theta} \\ \ddot{\phi} \end{bmatrix} = \begin{bmatrix} a1(\theta, \phi) & b1(\theta, \phi) \\ a2(\theta, \phi) & b2(\theta, \phi) \end{bmatrix}^{-1} \begin{bmatrix} c1(\theta, \phi, \dot{\theta}, \dot{\phi}) \\ c2(\theta, \phi, \dot{\theta}, \dot{\phi}) \end{bmatrix} = \begin{bmatrix} A(\theta, \phi, \dot{\theta}, \dot{\phi}) \\ B(\theta, \phi, \dot{\theta}, \dot{\phi}) \end{bmatrix}$$

Therefore, the differential equations of motion could be expressed in the state-space form

$$\frac{d}{dt} \begin{bmatrix} \theta \\ \dot{\theta} \\ \dot{\phi} \\ \ddot{\phi} \end{bmatrix} = \begin{bmatrix} \dot{\theta} \\ \dot{\phi} \\ A(\theta, \phi, \dot{\theta}, \dot{\phi}) \\ B(\theta, \phi, \dot{\theta}, \dot{\phi}) \end{bmatrix}. \quad (7)$$

Together with initial conditions, the dynamic motion of the R-SLIP model in the stance phase can be simulated numerically.

In the flight phase, the motion is ballistic and affected by gravity only, so the equations of motion can be described as

$$x_f = x_{LO} + \dot{x}_{LO}t$$

$$y_f = y_{LO} + \dot{y}_{LO}t - \frac{1}{2}gt^2, \quad (8)$$

where the subscript  $f$  and  $LO$  indicate the flight phase and liftoff, respectively.

### III. DYNAMICS OF THE R-SLIP MODEL

The R-SLIP model shown in (7) and (8) is a conservative system. Thus, the system dynamics in a full stride, including stance and flight phases, can be evaluated with pre-set four system parameters,  $(r, K_t, m, l)$ , and chosen initial system conditions. The initial system conditions are usually given at the moment of touchdown (i.e., begin of the stance phase), which includes model landing angle ( $\beta$ ), touchdown speed ( $V_{amp}$ ), and touchdown angle included by the touchdown velocity and horizontal line ( $\alpha$ ) as shown in Fig. 2(a). With these definitions, the initial system conditions can be converted to

$$\dot{x}_s = V_{amp}\cos(\alpha)$$

$$\dot{y}_s = V_{amp}\sin(\alpha)$$

$$\theta_{ini} = \pi - \phi_{ini} - \beta$$

$$\begin{bmatrix} \dot{\phi} \\ \ddot{\phi} \end{bmatrix} = \begin{bmatrix} -r(1 + \sin(\phi_{ini} - \theta_{ini})) - ls\sin(\theta_{ini}) & r(1 + \sin(\phi_{ini} - \theta_{ini})) \\ -rc\cos(\phi_{ini} - \theta_{ini}) + lc\cos(\theta_{ini}) & rc\cos(\phi_{ini} - \theta_{ini}) \end{bmatrix}^{-1} \begin{bmatrix} \dot{x}_s \\ \dot{y}_s \end{bmatrix}, \quad (9)$$

where subscript  $ini$  indicates the moment of touchdown. Please also note that  $\phi_{ini}$  is equal to  $\phi_0$  since the torsion spring is uncompressed in the flight phase. The converted parameters shown in (9) can be imported into (7) for simulation in the stance phase.

For stable running, at certain moment the system should change its status from the stance phase to the flight phase. The lift-off moment can be evaluated by the state of vertical body acceleration and velocity. If the above state meets the equations shown below

$$\ddot{y}_s = -g$$

$$\dot{y}_s > 0, \quad (10)$$

the system will lift-off. In addition, two necessary conditions should be satisfied for continuous running: (i) the horizontal velocity at lift-off is in the forward direction

$$\dot{x}_{LO} > 0, \quad (11)$$

and (ii) the height of the system at lift-off is high enough, so the follow-up touchdown with preset landing angle ( $\beta$ ) after ballistic flight is feasible

$$y_{LO} + \frac{\dot{y}_{LO}^2}{2g} > r + rs\sin(\beta). \quad (12)$$

In short, equation (10)-(12) are the essential criteria to grant the existence of next stance phase. Since the energy is conservative in flight phase as shown in (8) as well as the landing angle ( $\beta$ ) is preset, the touchdown speed ( $V_{amp}$ ) at every touchdown is the same. Moreover, the touchdown angle for the next stance phase can be defined as

$$\alpha = \arccos \left( \frac{\dot{x}_{LO}}{V_{amp}} \right). \quad (13)$$

By importing these values into (9) and then into (7), simulation of the next stance phase can be executed. With the same iteration method, the simulation of continuous running from stride to stride can be performed.

The R-SLIP model is numerically evaluated according to the method described above, and its stability is judged by whether the system can perform periodic locomotion with stance and flight phases without falling down, similar to the method reported in [21]. A specific number of strides is set as the threshold; if the system can run stably above this number, it is considered stable with this set of parameters. Since with high threshold, like 100 strides, the results are similar to about 25 strides; however the tendency of stability is not so clear, the threshold is set to 25 strides. As described in the first paragraph of this section, there are 4 system parameters and 3 initial conditions. While system parameters  $(r, m, l)$  are generally fixed in given systems, the last parameter  $K_t$  is usually reserved for system tuning. On the other hand, three initial conditions  $(\beta, V_{amp}, V_{ang})$  may be controlled during locomotion. The touchdown speed  $V_{amp}$  and touchdown angle  $\alpha$  are determined by lift-off conditions before this ballistic flight; therefore, they could be adjusted through leg control in the last stance phase. In addition, the landing angle  $\beta$  could be adjusted in the flight phase as long as the flying height is high enough for leg reconfiguration. As a result, in the simulation, system parameters  $(r, m, l)$  are set to the values accordingly to the hexapod robot in the lab ( $r = 60mm, m = 3.7/3 \cong 1.23kg, l = 68mm$ ) [22], and  $K_t$ , together with three initial conditions  $(\beta, V_{amp}, V_{ang})$ , are varied to check system stability. The varied ranges of these 4 variables are selected accordingly to the empirical system as well. The graphic presentation is suitable for at most two variables. Thus, among 4 factors in total,  $(K_t, \beta, V_{amp}, \alpha)$ , two factors are fixed and the other two are varied in each set of simulation, and there exist 6 sets of variations.

Figure 3 shows the simulation results of these 6 sets of variations and several characteristics can be observed. The color bar shown on the right side indicates the number of strides the system can perform before it fails. Figure 3(a) reveals that with fixed touchdown velocity ( $V_{amp}$  and  $\alpha$ ), the

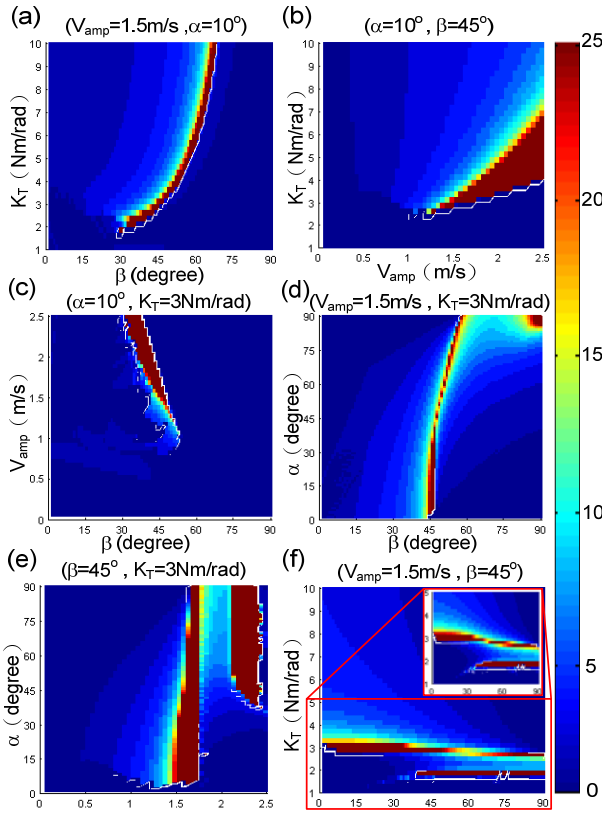


Fig. 3. Number of strides the system can run before failure. When the system can successfully run 25 strides, it is considered stable. There are 4 variables in total, ( $K_t$ ,  $\beta$ ,  $V_{amp}$ ,  $\alpha$ ). Thus, in each set of simulation (i.e., each figure) two factors are fixed and the other two are varied. There exist 6 sets of variations shown in (a)-(f), respectively. The fixed factors and their value are shown on top of each sub-figure, and the varied factors are simulated within the range shown in horizontal and vertical axes.

system could be stabilized by selecting the suitable landing angle, except for the system with very soft torsion spring. For the system with stiffer torsion spring, the larger landing angle is required. However, the stable region is very narrow. Any imperfect setting or disturbance would destabilize the system very quickly. Figure 3(b) shows that with fixed landing angle ( $\beta$ ) and relative angle of the touchdown velocity ( $\alpha$ ), the system is unstable for very soft spring or small touchdown velocity. The stiffer torsion spring also requires larger touchdown speed to stabilize the system, and the allowable range of speed increases as well. Figure 3(c) reveals that with fixed landing angle ( $\beta$ ) and stiffness of the torsion spring ( $K_t$ ), the system is unstable for small touchdown speed. With larger speed, the range of the landing angle for stable running is larger, but the angle should be decreased. Figure 3(d) shows that with fixed stiffness of the torsion spring ( $K_t$ ) and touchdown speed ( $V_{amp}$ ), the system can be stable with very precise mapping between the landing angle and relative angle of the touchdown velocity. Figure 3(e) indicates that with fixed landing angle ( $\beta$ ) and stiffness of the torsion spring ( $K_t$ ), the touchdown speed should be resided in two specific ranges to let the system stable. In addition, when this criterion is satisfied, the suitable range of the relative angle of the

touchdown velocity is very large. Figure 3(f) shows that with fixed touchdown speed ( $V_{amp}$ ) and landing angle ( $\beta$ ), the system can be stable with only very narrow range of spring stiffness. When the stiffness is right, the relative angle of the touchdown velocity can be varied in certain range. There exist two stable regions of parameters. The one with lower stiffness requires larger relative angle of the touchdown velocity. In contrast, the one with higher stiffness requires smaller relative angle of the touchdown velocity.

The touchdown speed ( $V_{amp}$ ) shown in Figure 3 is selected according to the measurements from the physical system. Because the selected values are just located on the edge of stable region as shown in Figure 3(b), it is intuitively that the stable region plotted in the other plots will be narrow. It also indicates that with higher touchdown speed and stiffer spring, the stable range might be larger. Therefore, the size of stable region is mainly decided by the collocation of stiffness of torsion spring and touchdown speed. The analysis described above shows that with predefined mass and radius of circular leg, the adequate touchdown speed and stiffness of torsion spring of the robot for stable locomotion can be roughly known from Figure 3(b) since the reasonable touchdown angle and landing angle are in small range. On the contrary, if the stable speed and stiffness are not available, the radius of circular leg may need to be adjusted. After the speed and stiffness have been decided, the precise stable landing angle and touchdown angle are not too hard to be found through simulation of Figure 3.

Though Fig. 3 provides the rough estimation of the system stability, how the states changes from strides to strides and the states at fixed point cannot be revealed. Therefore, the return map is utilized for further analysis. Because stiffness of the torsion spring, landing angle and touchdown speed may be easier to control than that of the touchdown angle, the return map is utilized to check the state transition of the touchdown angle with given other three factors ( $K_t$ ,  $\beta$ ,  $V_{amp}$ ). The results are shown in Fig. 4 (a)-(c), where in each sub-figure two of the factors are fixed and the other one is varied within certain range. Figure 4(a) plots the return maps with fixed landing angle and stiffness of the torsion spring, and the touchdown speed within range  $V_{amp} = 0.5 - 3.0 \text{ m/s}$  are varied with rough increment  $0.25 \text{ m/s}$ , wherein range  $V_{amp} = 1.5 - 2.5$  are selected to vary with fine increment  $0.1 \text{ m/s}$  because of the existence of stable fixed points. When the touchdown speed is low (i.e.,  $0.5 - 1.25$ ), the increment is about half to one fifth of touchdown speed, so the touchdown angle of next step with these speeds varies greatly. In the meantime, since the system does not have enough kinematic energy to roll over enough angles before lifts off, the touchdown angle of next step is too high for stable motion. Therefore, the trajectories don't cross the line which passes through the original with slope 1, and no fixed point exists. The results match the results shown in figure 3(e) as well. While the touchdown speed resides within  $1.5 - 1.7 \text{ m/s}$  and the energy of system is high enough, there exists a fixed point located around low touchdown angle. It is a stable fixed point

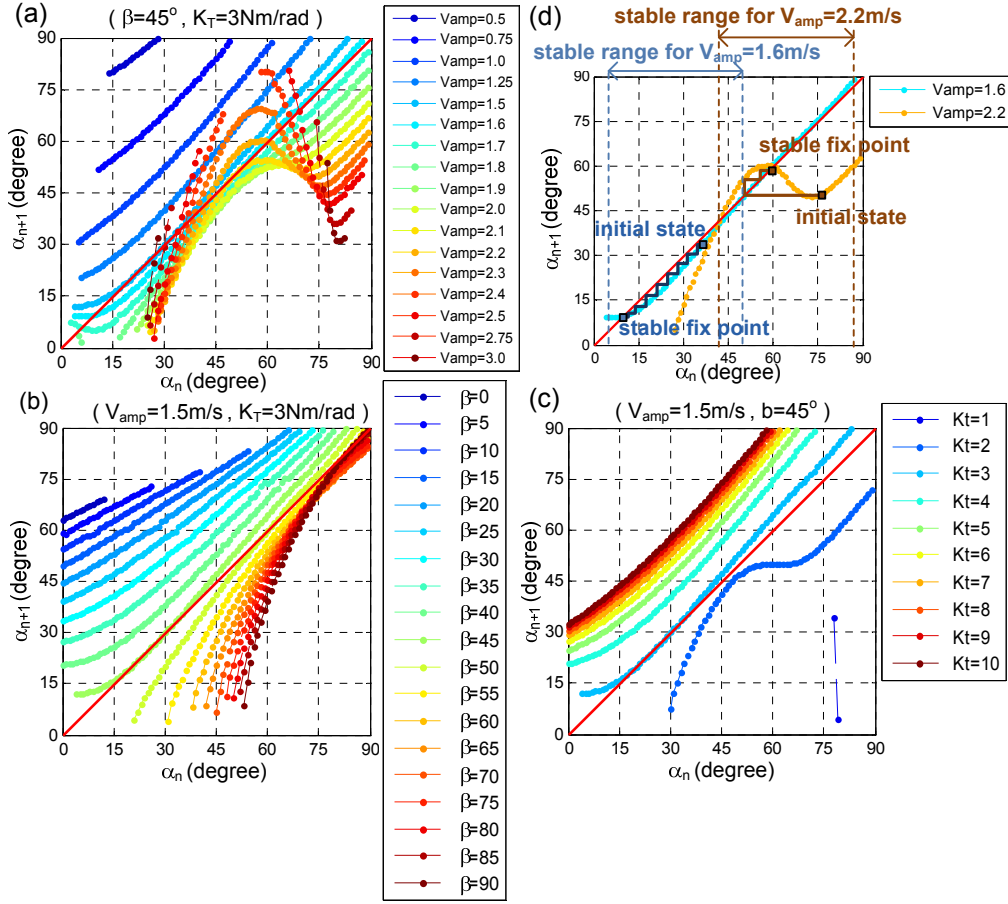


Fig. 4. The return map of the R-SLIP model: (a) Varying the amplitude of the touchdown velocity from 0.5 to 3.0 m/s; (b) varying the landing angle  $\beta$  from 0 to  $90^\circ$ ; (c) varying the stiffness of the torsion spring from 1 to 10 Nm/rad; (d) the stable fixed points.

since the slope of the trajectory around this fixed point is located between the interval  $[-1, 1]$ . For example, in the case of  $V_{amp} = 1.6$ , the stable range of the touchdown angle is within  $5 - 50^\circ$  as shown in Fig. 4(d). The system with the state near this fixed point would approach and stay around this stable fixed point. The stable region increases while the touchdown speed. While the magnitude of the touchdown velocity resides in  $1.8 - 2.0 \text{ m/s}$ , there is no fixed point and the system is unstable. While the magnitude of the touchdown velocity resides in  $2.1 - 2.2 \text{ m/s}$ , a stable fixed point appears again but located at higher relative angle of the touchdown velocity. For even higher magnitude, two fixed points exist, but none of them is stable. The return maps with varying landing angle ( $\beta$ ) and stiffness of the torsion spring ( $K_t$ ) are shown in Fig. 4(b) and 4(c). The first one fixes  $K_t$  and varies  $\beta = 0 - 90^\circ$  with increment  $5^\circ$ , and the second one fixes  $\beta$  and varies  $K_t = 1 - 10 \text{ Nm/rad}$  with increment  $1 \text{ Nm/rad}$ . Figure 4(b) shows that the large landing angle would lead to a large touchdown velocity angle in substance, and with a correct landing angle, the system with small touchdown angle can be stabilized owing to the existence of the stable fixed point. In contrast, the system with large touchdown angle cannot be stabilized by any landing angle, except for the  $90^\circ$  case, where the system

behaves like a 1-dimensional hopper moving vertically. In reality, however, the circular legs may not behave well with high touchdown speed and large touchdown angle since the large deformation may fatigue the empirical legs. Figure 4(c) reveals that the effect of stiffness of the torsion spring on stability is similar to that of touchdown speed. The effect of increasing touchdown speed is in certain level equivalent to decreasing stiffness of the torsion spring since the ratio of them relates to the exchange of kinematic and potential energy of system and the exercise of system is just the process of it. The touchdown speed represents the amount of kinetic energy preserved in the system. In contrast, the stiffness of the

torsion spring represents how much and how quick the energy can be stored in the spring potential. Thus, for a system with given mass, intuitively these two factors should be matched in certain range to let the system run continuously. On the other hand, the landing angle and touchdown angle would also affect how much kinematic energy transfer to potential energy and the lift-off velocity angle. The lift-off velocity angle decides the touchdown angle of next step; so a well tuned landing angle makes touchdown angle converge to a fixed number and let system stable. Furthermore since the touchdown speed directly determines the energy of system but the landing angle and stiffness of spring are just about the energy transformation, the tendency of return map with different speed change more rapidly than with different landing angle and stiffness of spring.

The return map shown in figure 4 reveals that the R-SLIP model has “self-stable” gaits, just like the traditional SLIP model reported in [23]. With adequate initial conditions,  $(\beta, V_{amp}, \alpha)$ , and system parameters,  $(r, K_t, m, l)$ , the system can run stably at the fixed point without control effort. Thus, if the robot can be operated to run within the self-stable region, the required power input would be merely for overcoming the mechanical damping and disturbance from environment. It can run very efficiently. The results shown in Fig. 4 indicate

that stable range in touchdown speed and touchdown angle is wide, especially the latter one. Thus, if the touchdown speed (i.e.,  $V_{amp} = 1.7\text{m/s}$ ) is controlled perfectly, the stable range of the touchdown angle can be spanned as wide as  $80^\circ$ . This is one of the special characteristics the traditional SLIP model doesn't have. Because the touchdown angle is the hardest to control, this characteristic is indeed advantageous. In addition, the touchdown speed can be adjusted by actively change the rotating speed of the legs in the stance phase. Though it might be hard to be controlled precisely, the stable running is still feasible since the stable region of the touchdown speed is not small. On the other hand, the control of the landing angle is the most crucial one since its stable region is small. Nevertheless, it is also the easiest to control by leg positioning in the flight phase.

#### IV. CONCLUSION

We report on the development of the model for running locomotion with rolling contact, R-SLIP, to simulate the motion of the robot with circular legs. Thus, two significant characteristics which cannot be correctly modeled in the traditional SLIP, rolling contact with varied equivalent linear spring during locomotion, can be adequately captured. The dynamic equations of the model were derived based on the Lagrangian method. Then, the stability of the R-SLIP model was analyzed numerically by varying the factors which affects the dynamic performance of the systems, including one system parameter, stiffness of the torsion spring, and three initial conditions, including touchdown angle, touchdown speed, and landing angle. In addition, the return map was utilized to check the state transition of the touchdown angle with given other three factors. The results reveal that the R-SLIP model has self-stable gaits (i.e., with stable fixed points), just like the traditional SLIP. Thus, with adequate initial conditions and system parameters, the system can run stably around the fixed point without control effort.

We are currently in the process of analyzing the performance similarity and difference between the empirical high-order circular leg and the reduced-order R-SLIP model, so the realization of the model onto the real robot can be more realistic. In parallel, we are also trying to directly implement the stable gait of the R-SLIP model onto the hexapod robot, to evaluate the performance of the model experimentally.

#### REFERENCES

- [1] R. M. Alexander, *Elastic mechanisms in animal movement* Cambridge University Press 1988.
- [2] R. Blickhan, "The spring mass model for running and hopping," *Journal of Biomechanics*, vol. 22, pp. 1217-1227, 1989.
- [3] P. Holmes, R. J. Full, D. Koditschek, and J. Guckenheimer, "The dynamics of legged locomotion: Models, analyses, and challenges," *Siam Review*, vol. 48, pp. 207-304, Jun 2006.
- [4] I. Poulakakis and J. W. Grizzle, "The Spring Loaded Inverted Pendulum as the Hybrid Zero Dynamics of an Asymmetric Hopper," *Ieee Transactions on Automatic Control*, vol. 54, pp. 1779-1793, Aug 2009.
- [5] M. M. Ankarali and U. Saranli, "Control of underactuated planar pronging through an embedded spring-mass Hopper template," *Autonomous Robots*, vol. 30, pp. 217-231, Feb 2011.
- [6] R. J. Full and D. E. Koditschek, "Templates and anchors: Neuromechanical hypotheses of legged locomotion on land," *Journal of Experimental Biology*, vol. 202, pp. 3325-3332, Dec 1999.
- [7] M. H. Raibert, "Hopping in legged systems - modeling and simulation for the two-dimensional one-legged case," *IEEE Transactions on Systems Man and Cybernetics*, vol. 14, pp. 451-463, 1984.
- [8] I. Poulakakis, J. A. Smith, and M. Buehler, "Modeling and experiments of untethered quadrupedal running with a bounding gait: The Scout II robot," *International Journal of Robotics Research*, vol. 24, pp. 239-256, Apr 2005.
- [9] H. Kimura, Y. Fukuoka, and A. H. Cohen, "Adaptive dynamic walking of a quadruped robot on natural ground based on biological concepts," *International Journal of Robotics Research*, vol. 26, pp. 475-490, May 2007.
- [10] S. Kim, J. E. Clark, and M. R. Cutkosky, "iSprawl: Design and tuning for high-speed autonomous open-loop running," *International Journal of Robotics Research*, vol. 25, pp. 903-912, Sep 2006.
- [11] J. G. Cham, J. K. Karpick, and M. R. Cutkosky, "Stride period adaptation of a biomimetic running hexapod," *International Journal of Robotics Research*, vol. 23, pp. 141-153, Feb 2004.
- [12] J. G. Cham, S. A. Bailey, J. E. Clark, R. J. Full, and M. R. Cutkosky, "Fast and robust: Hexapedal robots via shape deposition manufacturing," *International Journal of Robotics Research*, vol. 21, pp. 869-882, Oct-Nov 2002.
- [13] R. Altendorfer, N. Moore, H. Komsuolu, M. Buehler, H. B. Brown, D. McMordie, U. Saranli, R. Full, and D. E. Koditschek, "RHex: A biologically inspired hexapod runner," *Autonomous Robots*, vol. 11, pp. 207-213, Nov 2001.
- [14] U. Saranli, M. Buehler, and D. E. Koditschek, "RHex: A simple and highly mobile hexapod robot," *International Journal of Robotics Research*, vol. 20, pp. 616-631, Jul 2001.
- [15] J. E. Clark, D. I. Goldman, P. C. Lin, G. Lynch, T. S. Chen, H. Komsuoglu, R. J. Full, and D. E. Koditschek, "Design of a bio-inspired dynamical vertical climbing robot," in *Robotics: Science and Systems*, Atlanta, 2007.
- [16] P. C. Lin, H. Komsuoglu, and D. E. Koditschek, "Sensor data fusion for body state estimation in a hexapod robot with dynamical gaits," *IEEE Transactions on Robotics*, vol. 22, pp. 932-943, Oct 2006.
- [17] P. C. Lin, H. Komsuoglu, and D. E. Koditschek, "A leg configuration measurement system for full-body pose estimates in a hexapod robot (vol 21, pg 411, 2005)," *IEEE Transactions on Robotics*, vol. 21, pp. 778-778, Aug 2005.
- [18] S. Burden, J. Clark, J. Weingarten, H. Komsuoglu, and D. Koditschek, "Heterogeneous Leg Stiffness and Roll in Dynamic Running," in *Robotics and Automation, 2007 IEEE International Conference on*, 2007, pp. 4645-4652.
- [19] P. C. Lin, "Proprioceptive sensing for a legged robot," Ph.D. Dissertation, University of Michigan, 2005.
- [20] J. Jae Yun and J. E. Clark, "Effect of rolling on running performance," in *Robotics and Automation (ICRA), 2011 IEEE International Conference on*, 2011, pp. 2009-2014.
- [21] A. Seyfarth, H. Geyer, M. Gunther, and R. Blickhan, "A movement criterion for running," *Journal of Biomechanics*, vol. 35, pp. 649-655, May 2002.
- [22] K.-J. Huang, S.-C. Chen, and P.-C. Lin, "A Bio-inspired single-motor-driven hexapod robot with dynamical gaits," in *IEEE/ASME International Conference on Advanced Intelligent Mechatronics (AIM)*, 2012.
- [23] R. M. Ghigliazza, R. Altendorfer, P. Holmes, and D. Koditschek, "A simply stabilized running model," *Siam Review*, vol. 47, pp. 519-549, Sep 2005.